




Thermal History of Asteroid Parent Bodies Is Reflected in Their Metalorganic Chemistry

Marco Matzka¹, Marianna Lucio¹, Basem Kanawati¹, Eric Quirico³, Lydie Bonal³, Stefan Loehle⁴, and Philippe Schmitt-Kopplin^{1,2} 

¹ Research Unit Analytical BioGeoChemistry, Helmholtz Zentrum München, 85764 Neuherberg, Germany

² Analytical Food Chemistry, Technische Universität München, 85354 Freising-Weihenstephan, Germany

³ Institut de Planetologie et Astrophysique de Grenoble, University Grenoble Alpes, 38058 Grenoble, France

⁴ High Enthalpy Flow Diagnostics Group (HEFDiG), Institute of Space Systems, Stuttgart, Germany

Received 2021 April 1; revised 2021 May 31; accepted 2021 June 1; published 2021 June 30

Abstract

Organo-magnesium compounds were shown to contribute significantly to the soluble carbon molecular complexity and diversity of meteorites, and their analysis increases our knowledge on carbon stabilization/sequestration processes in the asteroidal parent body. Here we present a new group of sulfur-magnesium-carboxylates detected using ultra-high-resolution mass spectrometry in a variety of meteorites. These novel compounds show increased abundance correlated with the thermal history of the asteroid parent bodies. By comparing the soluble organic extracts of 44 meteorites having experienced variable post-accretion history, we describe distinct organic compound patterns of sulfur-magnesium-carboxylates in relation to their long- and short-duration thermal history. It is shown that the exceptional stability of these molecules enables survival of carbon under harsh thermal extraterrestrial conditions, even in the vitrified fusion crust formed during entry into the Earth's atmosphere. Sulfur-magnesium-carboxylates augment our understanding of parent body proceedings with regard to carbon sequestration and speciation in space.

Unified Astronomy Thesaurus concepts: Asteroids (72); Meteorite composition (1037); Meteorites (1038); Carbonaceous chondrites (200); Achondrites (15); Astrobiology (74); Carbon-nitrogen cycle (194); Chemical enrichment (225)

1. Introduction

Meteorites not only consist of mineral and inorganic metal phases but also embody an immense diversity of carbon-based chemistry. These organic compounds were reported in many extraterrestrial samples, including various carbonaceous, ordinary chondrites, as well as achondrites, such as HED (howardite-eucrite-diogenite) meteorites (Pizzarello et al. 2006; Schmitt-Kopplin et al. 2010; Popova et al. 2013; Unsalan et al. 2019). Various life-relevant organic compounds such as the high variety of amino acids (Kvenvolden et al. 1971; Cronin & Pizzarello 1983), nucleobases (Martins et al. 2008; Callahan et al. 2011), carbohydrates (Furukawa et al. 2019), fatty acids (Lawless & Yuen 1979), and inorganic gases (Srinivasan & Anders 1978) have generally been detected and analyzed in meteorites. The CM2 meteorite Murchison, a carbonaceous chondrite breccia from the Mighei type with alteration by water-rich fluids on its parent body, is still being intensively investigated since its fall in 1969 and considered as a well-known extraterrestrial sample for abiotic organic complexity (Anders 1971; Laurretta & McSween 2006). Recently, nontargeted organic spectroscopy involving ultra-high-resolution methods in mass spectrometry and nuclear magnetic resonance spectroscopy expanded the structure description of the soluble organic matter of such valuable meteorites (Naraoka et al. 2017; Hashiguchi & Naraoka 2019). The access to high-resolution analytical information using these novel technologies enables fundamentally new ways to identify and characterize the organic variety in extraterrestrial samples, containing not only carbon (C), hydrogen (H), and oxygen (O) but also a continuum of

heteroatoms such as nitrogen (N) and sulfur (S) and metal ions (Schmitt-Kopplin et al. 2010; Hertkorn et al. 2015; Hertzog et al. 2019).

Over the past decade, metal-containing organic molecules have been proven to be important in meteorites. These molecules are, for example, an iron-cyanide compound with similarity to the active site of hydrogenases (Smith et al. 2019; McGeoch et al. 2020) and a new class of dihydroxymagnesium carboxylate compounds, found in relation to strong metamorphic events in meteorites (Ruf et al. 2017). Light elements such as nitrogen (N) or sulfur (S) were detected in extraterrestrial meteoritic samples in different quantities and qualities in the form of gas to more complex molecular compounds (Botta & Bada 2002). Sulfur is especially known to be available in relatively high amounts as minerals such as pyrrhotite and pentlandite, as metal sulfides, and as organic molecules in various meteorites (Kaplan & Hulston 1966; Tenailleau et al. 2006; Schmitt-Kopplin et al. 2010). This element was found under different oxidation states, as well as in different compound classes such as sulfides (e.g., H₂S), mono- and disulfides, heterocycles, sulfoxides, sulfites, sulfones, sulfonates, and sulfates (Orthous-Daunay et al. 2010). Water alteration can mobilize sulfur from the mineral phases and from metal sulfides, which then can be subject for subsequent reactions (Schmitt-Kopplin et al. 2010). Furthermore, heating and shock can also release sulfur-containing structures from the insoluble organic matter. Under high pressure and temperature conditions, sulfur in its various oxidation states can interact with metals and carbonaceous phases to form thermodynamically stable compounds, which will be thermodynamically stable and survive the harsh extraterrestrial conditions. Discussed reactions to geosynthesize organic compounds in meteorites are Fischer-Tropsch-type (FTT) reactions (Masters 1979) or Sabatier processes (Sabatier 1913; Leonzio 2016), which use CO and H₂ in



Original content from this work may be used under the terms of the [Creative Commons Attribution 4.0 licence](https://creativecommons.org/licenses/by/4.0/). Any further distribution of this work must maintain attribution to the author(s) and the title of the work, journal citation and DOI.

proximity to catalytic mineral phases to form carbon chains, which can undergo further reactions.

In this study, we demonstrate the existence of a yet-unrecognized and novel organic compound class bearing the elements carbon, hydrogen, oxygen, sulfur, and magnesium—CHOSMg compounds. CHOSMg compounds are molecules with the general formula $C_xH_yMg_{1-2}O_zS_i$ with $x, y, z, i \in \mathbb{N}$. In the first part, we present structural and chemical properties of these CHOSMg compounds. We show that their formation is strongly dependent on the heating history of the fragment. This result is derived from the comparison of the inner matrix with crust material of the same meteorite. Finally, we show a correlation of CHOSMg compounds and the asteroid parent body temperature histories within a larger set of meteorite samples.

2. Results and Discussion:

2.1. Description of the CHOSMg Space

We analyzed the methanol soluble fraction from 44 meteorites from different classes using direct injection electrospray ionization Fourier transform ion cyclotron resonance mass spectrometry (ESI-FT-ICR-MS). Besides the known compositional organic content of the chemical families CHO, CHNO, CHOS, CHNOS, and CHOMg as described previously in meteoritic organic material (Schmitt-Kopplin et al. 2010), many signals were not covered by these compositional assignments. Using a combination of the elements C, H, O, S, and Mg enables the assignment of these signals to a new chemical family never described to date, CHOSMg. These CHOSMg compounds, together with their isotopic signature, ESI-FT-ICR-MS, and mass spectra of four representative meteorites, are illustrated in Figure 1: an ordinary chondrite (LL5, Chelyabinsk; Popova et al. 2013), a magnesian mafic silicates-rich ungrouped achondrite (NWA 7325; Ruf et al. 2017), a heated anomalous CM2 chondrite (CM2-an, Diepenveen; Langbroek et al. 2019), and a moderately altered CM2 (CM2, Aguas Zarcas; Aponte et al. 2020; see also Figure A1 in the Appendix).

NWA 7325 (achondrite-ungrouped) presents 12% CHOSMg compounds in the SOM (Figure 1(A)). In Chelyabinsk (LL5), which experienced a heating history, CHOSMg compounds account for 15% of all assigned mass signals. Also, Diepenveen meteorite (CM2-an), which experienced extensive heating as seen from its petrology and organic molecules (Langbroek et al. 2019), constitutes 17% CHOSMg peak. In Diepenveen, the most intense signals in the spectra could be assigned to CHOSMg compounds. Even though Diepenveen shows a similar profile of organic compounds to thermal stressed Y793321 (CM2; Langbroek et al. 2019), the amounts of CHOSMg compounds in Y793321 are only 4.6%. Aguas Zarcas (CM2, which fell in 1919) saw only low temperatures, similar to CM2 Murchison (Van Schmus & Wood 1967; Aponte et al. 2020). Even though Aguas Zarcas contains an above-average amount of sulfur compared to other CM2 meteorites, with a diverse and complex CHOS chemical space (data not shown), only 1% of all annotations are CHOSMg compound.

To unambiguously assign CHOSMg elemental compositions from exact mass values, ultrahigh mass resolution techniques like FT-ICR-MS were needed. The combined resolving power of $R > 400,000$ at m/z 400 and a mass precision of <200 ppb allow for an unambiguous chemical formula assignment owing to high mass accuracy, which can distinguish compounds by the precision

of half a milli-atomic mass unit (mass of an electron; Schmitt-Kopplin et al. 2010; Smith et al. 2018). Furthermore, this high mass accuracy enables the detection of isotopologues of compounds if the natural abundance of the monoisotopic signal is sufficient. The isotope patterns as seen in the mass spectra are used to qualitatively confirm the assigned chemical composition by comparing the experimental results to a theoretical isotope pattern (Figures 1(C) and (D)). Mass peak $375.16969 \text{ m/z}^{-1}$ with the assignment $C_{16}H_{32}MgO_6S$ shows characteristic ^{25}Mg and ^{26}Mg isotope signatures and ^{34}S , ^{13}C , and ^{18}O peaks, as well as signals of their combinations with the intensity representative of their natural abundance.

2.2. Chemical Structure of CHOSMg

The profiles of CHOSMg compounds in the ungrouped achondrite NWA 7325 were further visualized in adapted van Krevelen diagrams (Figure 2). The complex and ordered chemical space of CHOSMg compounds covers a wide mass range between 200 and 700 m/z^{-1} with H/C values between 2.5 and 1 (Figure 2(A)). Most of the CHOSMg compounds contain one sulfur atom and show mostly complete methylene-based homologous CH_2 -series. Intensities are fairly similarly distributed over even and uneven carbon numbers, which validates an abiotic origin (Wakil 1989; Summons et al. 2008). Figure 1(B) displays a zoomed-in area from panel (A). Most of the CHOSMg compounds belong to series that elongate by CH_2 units and differ by the amounts of oxygen, hydrogen, and sulfur. The theoretical pathway to obtain CHOSMg compounds thus involves a step either to formally add MgO_4S to CHO compounds or to formally add SO_2 with loss of H_2 to CHOMg compounds. By comparing the fatty acid chains of CHO, CHOMg, and CHOSMg compounds in NWA 7325, it can be seen that more than half of the CHOSMg compounds share their fatty acid chains with either CHO compounds, CHOMg compounds, or both (Figure 2(C)). CHOSMg compounds are closely related in their chemical structure to CHO and CHOMg compounds and may represent either an endpoint or an intermediate product in the chemical evolution and stabilization of carbon in asteroid parent bodies. Most detected CHOSMg molecules contain six oxygen atoms as seen in Figure 2(D), two oxygens more than the CHOMg previously described by Ruf et al. (2017). They account for more than 1/3 of all CHOSMg compounds and are closely followed by CHOSMg molecules with five or seven oxygen atoms. As also seen in CHOMg compounds, principal chemical structures that exist in larger numbers than the others are probably the most stable ones (Ruf et al. 2017). Thus, it is to be expected that CHOSMg compounds with six oxygen atoms have characteristics that lead to the highest stability.

The CHOSMg compounds seem closely related in composition to CHO and CHOMg compounds and need some form of sulfur and magnesium to be generated. Sulfur is ubiquitous in its various oxidation states and is readily available in meteorites in mineral, (poly)sulfates/(poly)sulfides, and organic sulfurized molecules (Orthous-Daunay et al. 2010). Magnesium ions from the magnesium silicates matrices have been hypothesized to be involved in CHOMg compounds in interaction with existing carboxylic aliphatic acids (Ruf et al. 2017). Equally likely is the formation of coordination complexes with liberated sulfur from sulfate minerals attached to magnesium ions before or after the complexation with the carboxylate group of CHO compounds. Oxidation reactions to form an $\text{H}_2\text{MgO}_6\text{S}$ head group from lower oxidized sulfur species are plausible.

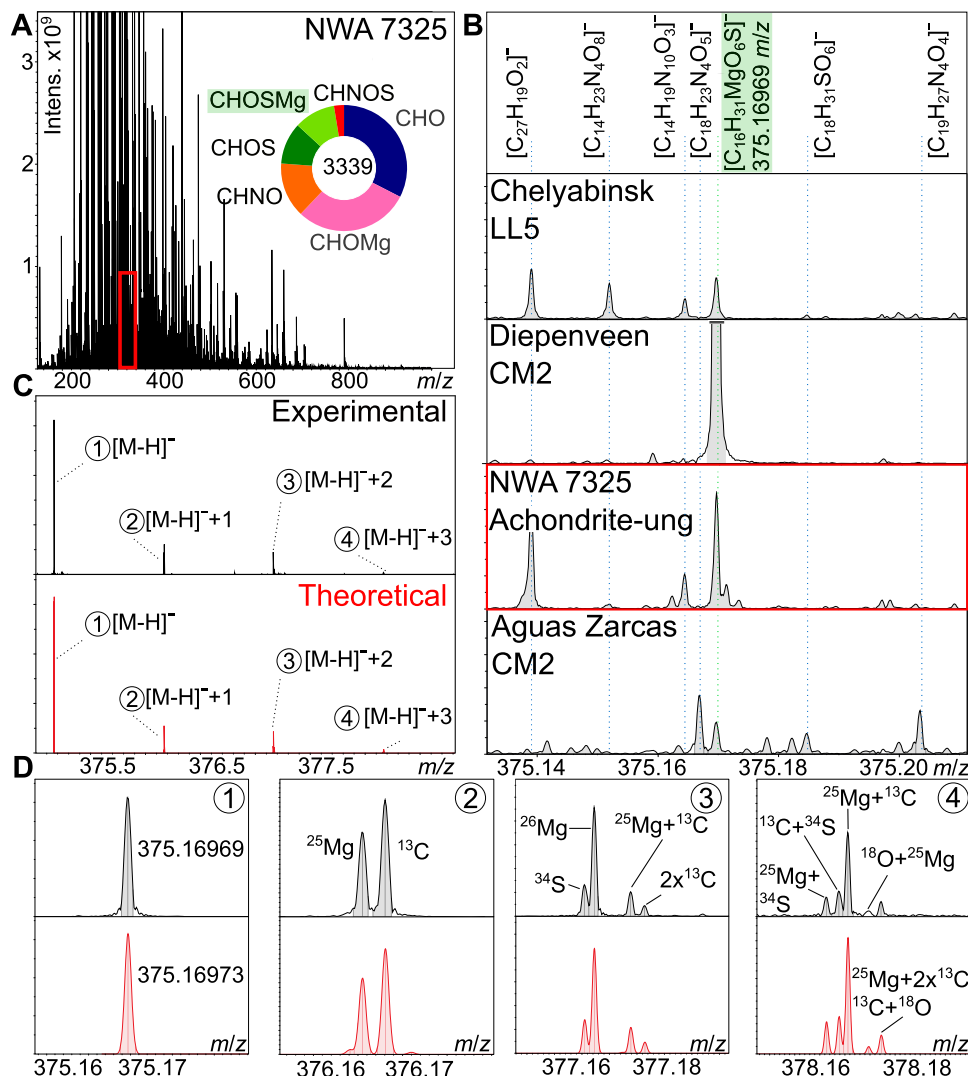


Figure 1. Detection of the CHOSMg compounds. (A) Negative electrospray ionization (ESI) Fourier transform ion cyclotron resonance mass spectrometry (FT-ICR-MS) mass spectrum of ungrouped achondrite NWA 7325 is shown. The donut plot shows the distribution over all chemical spaces, including the newly detected CHOSMg compounds in light green. The red box is enlarged in panel (B) under the name NWA 7325. (B) Comparison of the mass peak m/z 375.16969 assigned to monoisotopic formula $[C_{16}H_{31}MgO_6S]^-$ in ordinary chondrite Chelyabinsk (LL5), in ungrouped achondrite NWA 7325, and in carbonaceous chondrites Diepenveen (CM2-an) and Aguas Zarcas (CM2). Green color represents a chosen CHOSMg peak. The red box is the enlarged region from panel (A). (C) Comparison between the experimental and theoretical isotope pattern of m/z 375.16969 from panel (B) as the monoisotopic peak (^{12}C , ^{24}Mg , ^{32}S , ^{16}O , 1H). The given m/z value is from the respective highest isotope peak of each nominal mass. (D) Zoomed-in view of panel (C). Experimental and theoretical masses of isotope peaks are given. Isotope composition is specified in the experimental (upper) section of panel (D). Intensity scaling of spectra with shared x-axis is similar and thus allows comparison.

Both the emergence of CHOSMg compounds from CHO and CHOMg compounds are chemically achievable. A mass difference network analysis (see Figures 3(A) and (B)) shows a close connectivity between the CHO, CHOMg, and CHOSMg compounds, as they are systematically linked to each other with the same mass transitions. CHOMg compounds and CHOSMg are proposed to have structural similarities (see Figures 3(C) and (D)) because they share similar chemical stability to that in fragmentations by tandem mass spectrometry experiments, as well as in their rapid degradation at low pH. The common moiety of all organosulfur magnesium fragments detected in tandem mass spectrometry was found to be MgO_6S as a head group after various aliphatic chain fragmentation (see Figure A2 in the Appendix). The investigated peak of m/z 263.04448 m/z^{-1} shows decreasing intensities with increasing fragmentation energy. Detected fragments contain the stable sulfur-magnesium head group and a shortened carbon backbone. Ultimately, the shortest possible fragment of solely the sulfur-magnesium head group

without hydrocarbon chain attached was also detected through the fragmentation experiments. To confirm the proposed structural formula, the stability of $CHMgO_6S$ was calculated on the B3LYP/6-31+G(d,p) level of theory and given in Hartrees as seen in the Appendix (Figure A3). Harmonic frequency analysis calculations performed on two anionic optimized structures confirm that both shown anions represent energy minimums. The proposed structure from Figure 3(D) represents the more likely isomer and also shows similar geometrical features to those observed in CHOMg compounds. Due to its noticeable stability, it is not possible to observe MgO_2 , SO_2 , SO_4 , or $MgSO_4$ losses in fragmentation experiments (see Figure A2).

2.3. Temperature-induced Formation and Stability of CHOSMg

In contrast to many thermally altered meteorites, Murchison (CM2) barely contains compounds belonging to the CHOSMg

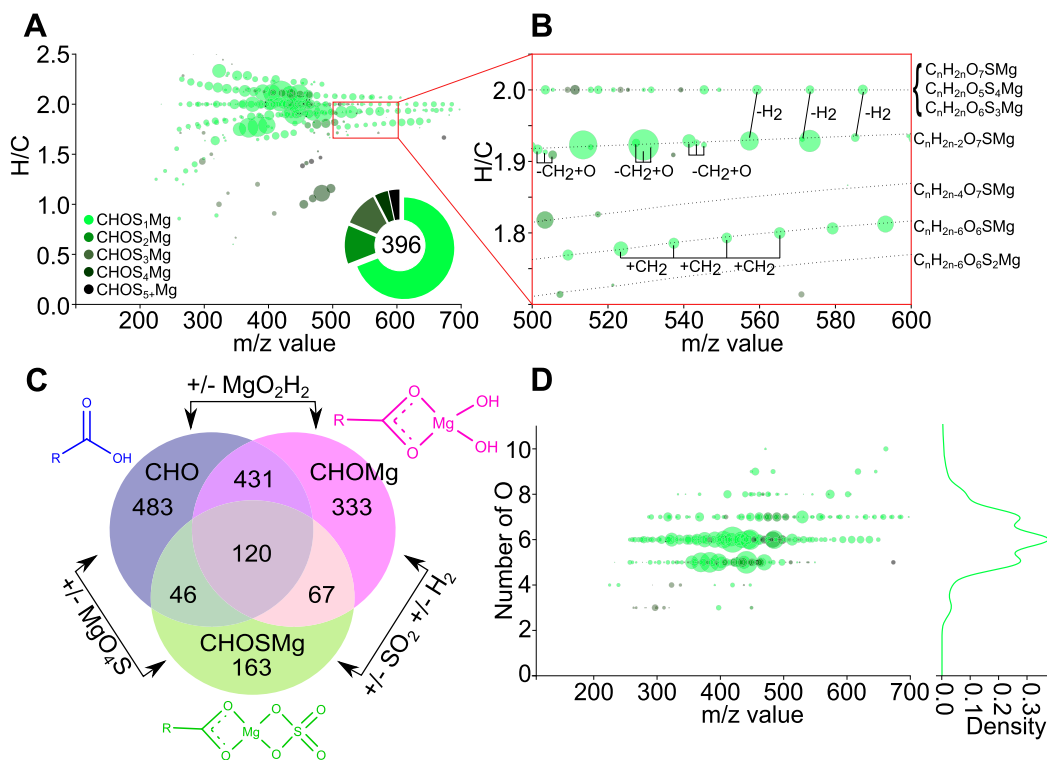


Figure 2. Characteristics of CHOSMg compounds of ungrouped achondrite NWA 7325 soluble organic matter analyzed with (-)ESI-FT-ICR-MS. (A) Mass-edited—H/C ratio diagram of CHOSMg compounds. Bubble size represents the intensity in the mass spectrum; color represents the amount of sulfur per CHOSMg compound according to the legend. The donut plot shows the total amount of CHOSMg compounds and shares of each of the five colored groups according to the legend. (B) Zoomed-in area from panel (A) with annotated homologous series and mass differences between the compounds. Methylene-based mass differences are marked by dotted lines. Examples for other mass differences than methylene-based ones are shown. Suggested chemical assignments of homologous series are depicted next to panel (B). (C) Venn diagram comparing the composition of fatty acid chain groups (“R”) of CHO (blue), CHOMg (magenta), and CHOSMg (green) compounds. Numbers in the Venn diagram are counts of fatty acid chains with unique composition ($C_xH_yO_z$ with $x, y, z \in \mathbb{N}$). The chemical structure of head groups of CHO, CHOMg, and CHOSMg is displayed in their respective color with fatty chain marked as “R” in the structure. (D) Plot with m/z values vs. number of oxygen. Bubble size and color according to panel (A). Density plot on the right side displays relative abundance of compounds with specific number of oxygen.

class. By heating Murchison under secondary vacuum (~ 10 – 5 mbar) to elevated temperatures for several hours, an increase of CHOSMg and CHOMg compounds was observed. At lower temperatures (lower 250°C), Murchison developed a large and complex chemistry regarding CHOSMg and CHOMg compounds. The CHOSMg compounds show a wider variation regarding aromaticity and oxygenation. Consequently, they are more easily generated and show higher abundance than CHOMg compounds (see Figure A4(C)). At high temperatures (600°C and above), the CHOSMg compounds reduced in number and complexity compared to lower 250°C samples, whereas CHOMg compounds stay fairly similar. Numbers of CHO, CHOS, CHOMg, and CHOSMg compounds (see Figure A5) show that short-time heating, e.g., triggered by impacts, reduces the amount of CHOS compounds that goes along with a liberation of, e.g., sulfates. These sulfates, as well as those from sulfur-containing minerals, allow the formation of CHOSMg compounds. However, at high temperatures, the sulfur from CHOSMg compounds is not stable enough to withstand the temperatures, but the more stable CHOMg compounds remain in the system. This can also be observed by the ratios of these compound families as seen in Figures A6 and A7. In a first step at 250°C , CHOSMg compounds are increasing over CHO compounds but decrease again at 600°C to 1000°C . CHOMg compounds behave fairly similar in terms of variation of abundances along temperature compared to CHOSMg compounds, but they increase at the highest temperature. Consequently, it can be assumed that CHOSMg

compounds are intermediate products during the formation of CHOMg out of CHO compounds regarding heat. This trend can also be observed by comparing the fusion crust and inner matrix of meteorites.

During atmospheric entry, the outer shell of meteorites reaches temperatures of more than 2000°C , resulting in melting and evaporation of the material. It is reported that the inner matrix stays relatively cold (Sears 1975). We compared the fusion crust and the core matrix of three different meteorites to assess the effect of temperature exposure on CHOSMg compounds. The separation between fusion crust and inner matrix was performed by physical force in an agate mortar. The heating during atmospheric entry eventually causes alteration of the carbon-containing compounds within the crust, which is seen in Figure 3. It is noteworthy that atmospheric entry is considered as heating only, neglecting the influence of pressure from the shock wave (Toppani et al. 2001). The analyzed meteorites were Aba Panu, a highly shocked (S4) L3 ordinary chondrite (Gattacceca et al. 2020), and the CM2s Aguas Zarcas, as well as Murchison. Panel (A) of Figure 3 shows the CHOSMg compounds in the respective inner matrix (top row) and the fusion crust (bottom row) of each of the three analyzed meteorites. Aba Panu contains a higher amount of CHOSMg compounds compared to Aguas Zarcas and Murchison. This might be related to higher extents of shocks of this meteorite. The CHOSMg compounds in Aguas Zarcas contain several sulfur atoms, which reflects the diverse sulfur chemistry in this meteorite. For Murchison, the amount of CHOSMg compounds

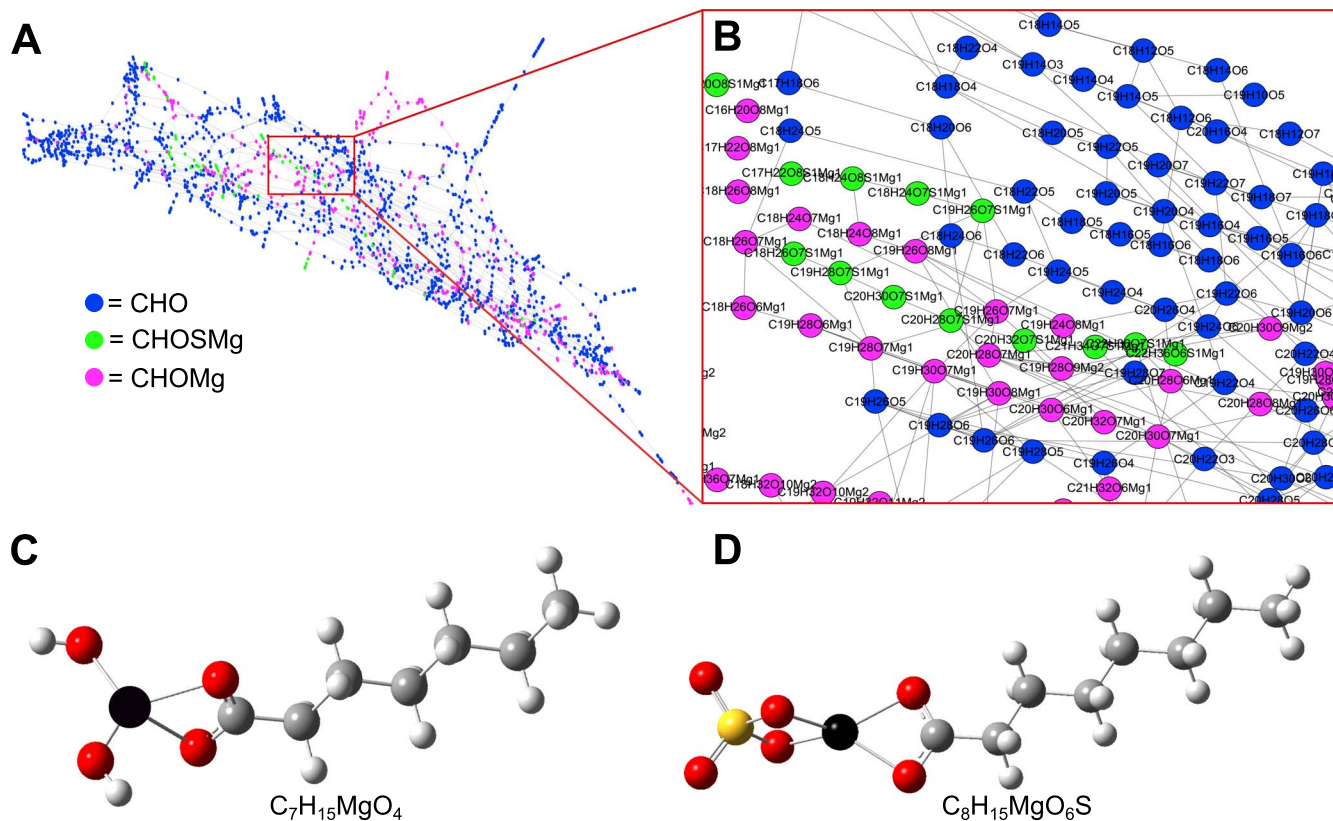


Figure 3. (A) Mass difference network of a heated Murchison sample (Murchison 250°C 3.5 hr) with (B) a zoomed-in view of a chosen position. Colored dots represent experimental masses and calculated elementary compositions of selected chemical spaces, CHO (blue), CHOSMg (green), and CHOMg (magenta). Lines between the dots present the mass differences H_2 , H_4 , CH_2 , C_2H_4 , O, H_2O , $MgSO_4$, MgH_2O_2 , S, S_2 , and Mg from a mass difference network analysis. (C) Proposed structure of CHOMg compounds as published (Ruf et al. 2017). (D) Proposed structure of CHOSMg compounds according to MS/MS experiments (see Figure A2) and stability calculations (see Figure A3). Colored dots represent carbon (dark gray), hydrogen (light gray), oxygen (red), magnesium (black), and sulfur (yellow).

is scarce, similarly to CHOMg compounds. All three meteorites show higher abundances of CHOSMg compounds in their fusion crusts than in their inner matrices. In the Aba Panu fusion crust, more than 75% of all CHOSMg compounds contain one sulfur atom. Compared to the Aba Panu inner matrix, the newly formed homologous series of CHOSMg compounds can be observed in the Aba Panu fusion crust (see Figure 3(A)). Aguas Zarcas also exhibits new homologous series in the fusion crust compared to its inner matrix. In the Aguas Zarcas fusion crust, a significant loss of sulfur atoms in CHOSMg can be observed in comparison to the Aguas Zarcas inner matrix. While the Aguas Zarcas inner matrix contained only 10% of $CHOS_1Mg$ compounds, the amount of $CHOS_1Mg$ rose to closely 75% in the fusion crust. The Murchison matrix contains hardly any CHOSMg compounds. And again, similarly to Aba Panu and Aguas Zarcas, a wide diversity and complexity of new CHOSMg homologous series are increased in the Murchison fusion crust compared to the inner matrix. The boxplots of Figure 4(B) show the amount of CHOSMg compounds in the matrix and crust of the three meteorites. Compared to the matrix, the average amount of CHOSMg compounds is higher in the fusion crust. Furthermore, the distribution of oxygen (Figure 4(C)) and of sulfur (Figure 4(D)) is different in the meteoritic fusion crust compared to the inner matrix. CHOSMg molecules in the matrix contain mostly six to eight oxygen atoms with only small differences to lower and higher amounts of oxygen. The amount of sulfur is similarly distributed over one to three sulfur atoms and shows a decrease beginning at four sulfur atoms. In fusion crust analysis, it was shown that the abundances of $CHMgO_6S$, $CHMgO_7S$,

and $CHMgO_8S$ are significantly increased compared to all other CHOSMg compounds. For sulfur in CHOSMg compounds in the crust, it can be seen that especially $CHOS_1Mg$ compounds are strongly increased and show a steady decrease with higher amounts of sulfur.

2.4. CHOSMg Compounds as a Surrogate Parameter for Temperature Incidents

We investigated a large number of meteorites (44) using partial least-squares discriminant analysis (PLS-DA) to describe structural correlations between thermal history and CHOSMg compounds. To assess the reliability of the PLS-DA, we tested the cross-validated predictive residuals through the analysis of variance. We observe a separation in three different groups, namely, a group with hydrothermal background without short-duration heating—T I (e.g., CM2 Paris), moderate short-duration heating—T II (e.g., C2 ungrouped Tagish Lake) and intense short-duration heating—T III\T IV (e.g., CR2 GRO 03116), and long-duration heating—LDH in meteorites (e.g., L6 Novato) (Bonal et al. 2016; Quirico et al. 2018, 2014). The plot in Figure 5(A) shows a thermal gradient from T I meteorites over T II, T III, and T IV meteorites to LDH meteorites going from left to right. Three regions in the plot were determined (see Figure 5(B)) and further used to evaluate the values of loadings that characterize all of those regions. Examples of the CHOSMg signature of each region are depicted in the Appendix (see Figure A9). Hydrothermal backgrounds without short-duration heating T I meteorites are mostly described by oxygen-rich CHOSMg compounds.

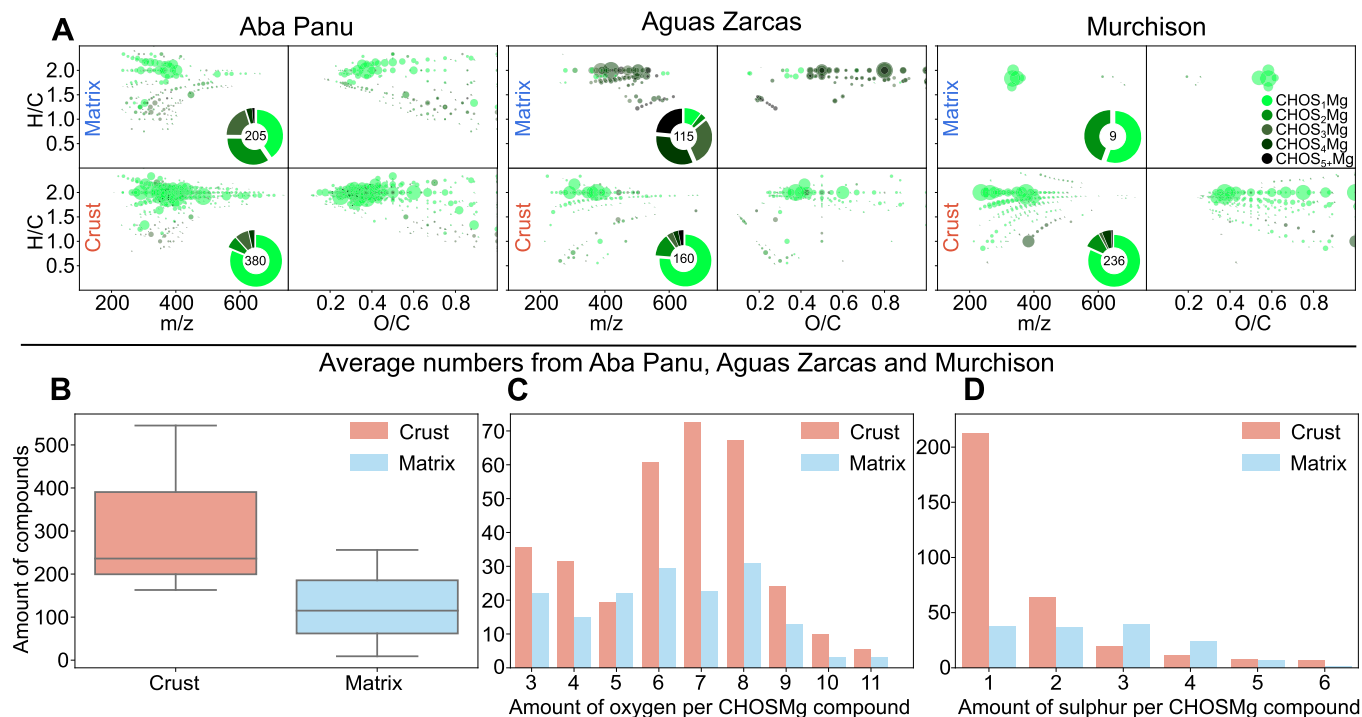


Figure 4. Difference between meteoritic matrix and fusion crust of three different meteorites. (A) Comparison between meteoritic matrix (top row) and meteoritic fusion crust (bottom row) of ordinary chondrite Aba Panu (L3) and carbonaceous chondrites Aguas Zarcas (CM2) and Murchison (CM2). Depicted are mass-edited H/C ratio diagrams (left side of each of the three panels) and O/C ratio vs. H/C ratio (van Krevelen) diagrams (right side of each of the three panels). Bubble size represents the intensity in the mass spectrum; color represents the amount of sulfur per CHOSMg compound according to the legend. The donut plot shows the total amount of CHOSMg compounds and shares of each of the five colored groups by count according to the legend. (B) Boxplot of the amount of CHOSMg compounds in the three meteorite samples, for crust (red, left side) and for matrix (blue, right side). (C) Average amount of oxygen per CHOSMg compound for crust (red) and matrix (blue). (D) Average amounts of sulfur per CHOSMg compound for crust (red) and matrix (blue). See also Figure A8.

Molecules with one sulfur are equally frequent as those with several sulfur atoms. Oxygen distribution (see Figure 4(C)) shows the highest amounts between seven and nine oxygen per CHOSMg compound. Notably, the O/C ratio of CHOSMg is very high compared to other compound classes owing to the fact that the magnesium-sulfur head group mostly incorporates six or more oxygen atoms, which results in high O/C ratio at low aliphatic acid chain lengths. CHOSMg compounds of more heated T II meteorites show higher contribution of sulfur atoms compared to the other regions. The oxygen numbers of T II meteorites are distributed similarly to the ones of T I meteorites. However, the number of sulfur atoms in T III/IV meteorites is strikingly high, which is also reflected in the low C/S ratio. Meteorites that experienced long-duration heating show a characteristic pattern of CHOSMg compounds. Approximately 75% of all compounds belong to CHOS₁Mg, 25% containing more than one sulfur atom. The CHOSMg compounds of this region are mostly carbon saturated compounds, and most of the compounds contain six or seven oxygen atoms, which has been shown to be a highly stable form of CHOSMg compounds (see Figure A3). Overall, the CHOSMg compounds show distinct characteristics according to the thermal history of the meteorite. Noteworthy is the fact that the amount of sulfur in CHOSMg compounds decreases with increasing heat. Our approach enables the discrimination between thermally stressed meteorites according to their CHOSMg signature, involving their information in carbon saturation and oxidation and the number of sulfur atoms. Some examples in predictions can be found in Figures A10 and A11 in the Appendix for Maribo CM2; low-temperature

meteorites Orgeil CI, Ivuna CI, Mundukpura CM2, and heated Diepenveen CM2; and DHO1988 CY in validation of our approach. This motivates us to consider many more meteorites and their whole CHNOSMg chemical space to set up heating prediction models that can find their application in the analysis of novel meteorite falls and return mission samples.

2.5. Conclusion and Outlook

In this work, we show the presence of a new and hitherto-undescribed carbon-based chemical compound class called CHOSMg compounds. These compounds are readily formed during temperature incidents. As their amount and chemical characteristics are different when looking at the inner matrix and the fusion crust of the same meteorite, we conclude that heat is an important factor of the formation of these magnesium organosulfur compounds. Moreover, by investigating a large set of meteorites, we describe that CHOSMg compounds follow meteorites according to their thermal history.

Our research reveals that hydrogen, carbon, oxygen, and magnesium, together with sulfur, are sequestered in thermostable metalorganic compounds in meteorites and can thus contribute to long-term astrochemical organic diversity. The extent of this formation is highly dependent on the thermal exposure of the asteroid parent body. The organic footprint in CHOSMg compounds in meteorites allows us to draw conclusions regarding the thermal history of the analyzed meteorites. While meteorites having witnessed only low-temperature exposures mostly contain CHOSMg compounds with higher amounts of oxygen and sulfur per molecule, the ones in more heated meteorites converge to a

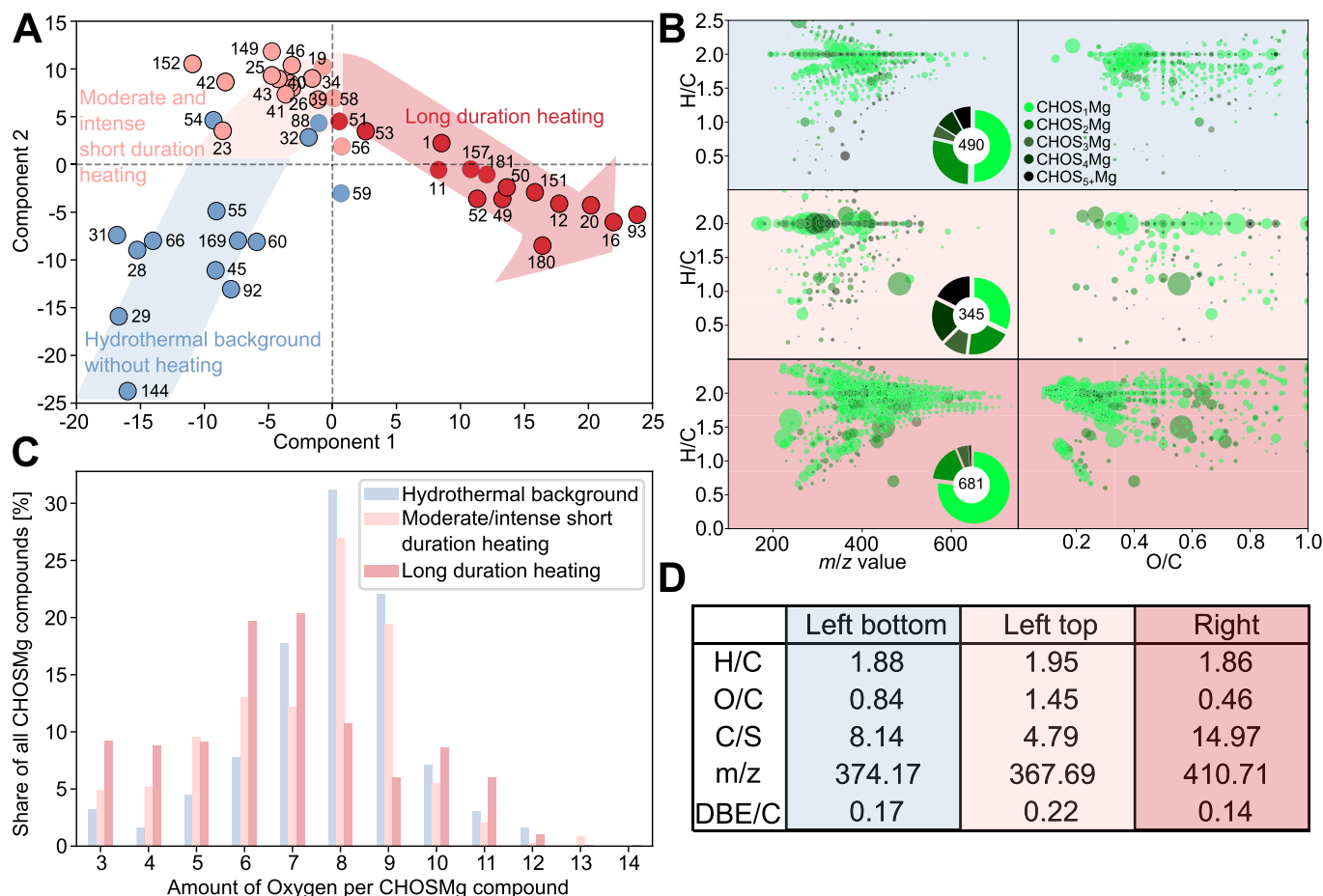


Figure 5. (A) PLS-DA of 44 different meteorites well described (Quirico et al. 2014; Bonal et al. 2016) regarding their thermal metamorphism history. Only CHOSMg compounds were used as PLS-DA loadings. Three categories were chosen according to the assigned thermal history. Hydrothermal background without short-duration heating (T I—dark blue), moderate short-duration heating (T II) and intense short-duration heating (T III/T IV—light red), and long-duration heating (LDH—dark red) (Quirico et al. 2018, 2014). Information on samples can be found in Table A1. Three areas of interest were marked in different background colors, namely, hydrothermal background without short-duration heating in light blue, moderate and intense short-duration heating in light red, and long-duration heating in dark red. (B) CHOSMg loadings of PLS-DA according to the three colored regions. Top row: hydrothermal background without short-duration heating in light blue; middle row: moderate and intense short-duration heating in light red; bottom row: long-duration heating in dark red. Depicted are mass-edited H/C ratio diagrams (left side of each of the three panels) and O/C ratio vs. H/C ratio (van Krevelen) diagrams (right side of each of the three panels). Bubble size represents the intensity in the mass spectrum; color represents the amount of sulfur per CHOSMg compound according to the legend. The donut plot shows the total amount of CHOSMg compounds and shares of each of the five colored groups according to the legend. (C) Amount of oxygen per CHOSMg compound vs. share of all CHOSMg compounds for the three colored areas of the PLS-DA, hydrothermal background without short-duration heating in light blue, moderate to intense short-duration heating in light red, long-duration heating in dark red. (D) Weighted averages of descriptive ratios for the three colored areas of the PLS-DA. Double bond equivalent (DBE) calculation is explained in the paragraph “material and methods.”

six-oxygen-bearing form (CHMgO₆S), which represents the most stable form of this compound class.

We show that the carbon-based CHOSMg molecules survive not only the harsh conditions of the asteroid parent body (extreme temperatures, pressures, and radiation) but also the atmospheric entry conditions where the material is heated to temperatures well above 2000°C in the meteorite crust. This illustrates the astrobiological impact of our study because these organic compounds in meteorites were continuously delivered to the early Earth’s surface through meteoritic impacts and still are. Due to their stability, the pool of CHOSMg compounds might have contributed significantly to the organic diversity found on Earth today. These might have played a significant role in the emergence of life on Earth as well. The organics in meteorites might have contributed to prebiotic chemistry and the formation of protocell membranes with their extreme chemical diversity and resilience toward heat more than thought so far, particularly in very primary hot periods on early Earth such as the Hadean.

Funded by the Deutsche Forschungsgemeinschaft (DFG, German Research Foundation)—Project-ID 364653263—TRR 235 (CRC 235).

Appendix Material and Methods

A.1. FT-ICR-MS

Five milligrams of each meteorite sample were washed three times with methanol in an agate mortar. Before crushing, 750 μ l methanol was added to the sample. The meteorite was further crushed until meteorite powder and methanol formed a homogeneous suspension. The suspension was transferred to an Eppendorf vial and left in an ultrasonic bath for 30 s. After centrifuging, the supernatant was transferred to another Eppendorf vial and ultimately used for ESI-FT-ICR-MS acquisition. The system was calibrated with L-Arginine clusters in negative mode. To ensure cleanness of the system, pure methanol blank spectra were acquired before measurement of

samples. Relevant peaks for this study are absent in methanol blanks.

A.2. Data Treatment

Spectra were internally calibrated with common fatty acids. Peaks were picked with signal-to-noise ratio of 3. All picked peaks were aligned respective to their m/z value with a 1 ppm error window. Assignment of elemental compositions was conducted with an in-house built software, NetCalc (Marianna et al. 2011). Only CHOSMg compounds were considered for further evaluation, which were present in more than 5% of the samples. These CHOSMg compounds were used for visual representation and statistical analysis.

A.3. FT-ICR-MS

Five milligrams of each meteorite sample were washed three times with methanol (Merck—Nr.106009) in an agate mortar. The washing methanol was disposed after each wash step to reduce contamination from handling. Before crushing, 750 μ l methanol was added to the sample. The meteorite was further crushed until meteorite powder and methanol formed a homogeneous suspension. The suspension was transferred to an Eppendorf tube (3810X; 1.5 ml) and left in an ultrasonic bath for 30 s. Subsequent to the ultrasonic bath followed centrifugation with a small table centrifuge. After centrifuging, the supernatant was transferred to another Eppendorf tube and ultimately used for ESI-FT-ICR-MS acquisition. The measurements were performed on a high-field Fourier Transform Ion Cyclotron Resonance mass spectrometer from Bruker Daltonics—Solarix. The magnet is a 12 T magnet from Magnex. Parameters were optimized with FTMS-Control V 2.2.0 from Bruker Daltonics. The mass spectra were acquired with a 4 megaword (MW) time domain. The system was calibrated with L-Arginine clusters in negative mode (5 mg L⁻¹ L-Arginine solved in methanol). To ensure cleanness of the system, pure methanol blank spectra were acquired before measurement of samples. Relevant peaks for this study are absent in methanol blanks. For each sample, scans were accumulated in the mass range of 122–1000 amu. Ions were accumulated for 300 ms in normal measurements mode and 1 s for MS/MS measurements. The pressure in the hexapole was 3×10^{-6} mbar, and the pressure in the ICR vacuum chamber was 6×10^{-6} mbar. As the source, we used the Apollo II (Bruker Daltonics), which is an ESI source. The supernatant from the extraction was directly injected via a microliter pump system (flowrate: 120 μ l h⁻¹). The source heating temperature was 200°C.

A.4. Data Analysis

All spectra were internally calibrated with a mass list of common fatty acids. Average errors of calibration were below 0.5 ppm. Peaks were picked with a signal-to-noise ratio of three. All peaks were aligned in a 1 ppm error window according to their m/z value. The elemental composition of all m/z values was calculated with an in-house built program, NetCalc (Marianna et al. 2011). Assignments were computed with an average accuracy window of ± 0.2 ppm. Only compounds that contain one Mg atom and one or more S atom were considered as CHOSMg compounds for further evaluation. CHOSMg compounds have to be present in at least 5% of the samples to delete unique annotations. The representation of the van Krevelen diagram and H/C-edited m/z diagram was used to visualize the

data. From the exact elemental compositions, the O/C and H/C ratio was calculated for each of the CHOSMg compounds. By plotting and comparing the O/C, H/C, and m/z values, the compounds can be characterized regarding saturation and oxidation levels (Van Krevelen 1950; Hertkorn et al. 2008).

A.5. Computations

The electronic structure calculations were performed on a server computer by running ab initio quantum mechanical computations, based on density functional theory (DFT), as implemented in Gaussian 09. The hybrid DFT-functional B3LYP was implemented with d-polarization functions for each heavy atom and 1 p for each hydrogen atom in all geometry optimization calculations with a 6–31+G(d,p) basis set. Frequency calculations were done for each optimized geometry with the same 6–31+G(d,p) basis set to obtain the zero-point vibrational energy. This value was multiplied by a scaling factor of 0.9804 to correct for vibrational anharmonicities. Another intention for performing the frequency analysis is the identification of transition states. Detecting imaginary frequencies implies that the optimized geometry is not fully relaxed as a stationary point (energy minimum) on the potential energy surface. The single-point energy calculations were done at the 6–311+G(d,p) level of theory. The use of diffuse functions was important to represent the correct geometry and thermodynamic properties of anionic species. Stability tests were performed to ensure that the used wave function represents the lowest-energy solution of the self-consistent field equations. For geometry optimization, the Berny analytical gradient optimization routines were used. The requested convergence value in the density matrix was 10^{-8} , the threshold value for maximum displacement was 0.0018 Å, and the threshold value for the maximum force was 0.00045 H B⁻¹. The nature of the stationary points was established by calculating and diagonalizing the Hessian matrix (force-constant matrix). All geometries of electronic structures calculated were viewed with the GaussView program (Dennington et al. 2003).

The network in Figure 3 was designed with Gephi version 0.9.2.

A.6. Statistical Evaluation

A total of 44 meteorites were aligned in a matrix, and the putative formulae were calculated with an in-house software (Marianna et al. 2011). We took into consideration the CHOSMg compounds detected in more than 5% of the meteorites. Signal intensities were normalized for each meteorite, dividing each peak intensity by the sum of all intensities of one measurement. We excluded from further elaboration the 10% highest and lowest intensities, to neglect extremely high and low values. The values were scaled by UV (unit variance) scaling. A principal component analysis (PCA) was applied to have an overview of the data. PCA analysis reduces the dimensionality of the data without losing important information. Ultimately, the analysis gives a representation of components that best describe the variance found in the data and separate samples accordingly. Furthermore, from metadata, we categorized the meteorites in three groups, namely, hydrothermal background without short-duration heating (TI), moderate short-duration heating (TII) and intense short-duration heating (TIII/TIV), and long-duration heating (LDH) (Quirico et al. 2018) (see Table A1). These data were analyzed with (PLS-DA) regressions models.

Table A1
Table of All Meteorite Samples Measured

ID	Meteorite	Type	Number of	Number of	Percent	Ratio	Ratio	Heating	Shock
Number	Description	Class	CHOSMg Formulae	Total Assignments	CHOSMg of Total	CHOSMg/ CHO	CHOMg/ CHOSMg	History	Status
152	Tagish Lake	C2-ung	353	6429	5.49	0.45	1.64	T II	1
19	Yamato 86720	C2-ung	516	11386	4.53	0.37	1.08	T III/T IV	4
32	MET 01070	CM1	36	8644	0.42	0.04	2.78	T I	...
23	Cold Bokkeveld	CM2	1587	16335	9.72	0.91	0.68	T II	1
25	EET 87522	CM2	294	1918	15.33	5.76	0.08	T II	...
26	EET 96029	CM2	104	1373	7.57	4.33	0.03	T II	...
31	MCY 05230	CM2	831	16272	5.11	1.07	0.05	T I	...
34	MIL 07700	CM2	227	4747	4.78	0.6	0.39	T II	...
39	PCA 02010	CM2	120	1521	7.89	2.79	0	T III/T IV	...
40	PCA 02012	CM2	118	1329	8.88	2.03	0.04	III/T IV	...
43	WIS 91600	CM2	771	3778	20.41	2.03	0.5	T II	...
45	Yamato 791198	CM2	818	14867	5.5	0.76	0.35	T I	...
46	Yamato 793321	CM2	163	3496	4.66	1.96	0.4	T II	...
66	DOM 08003	CM2	579	10141	5.71	0.85	0.11	T I	...
88	Murchison	CM2	9	13762	0.07	0.01	2.22	T I	2
92	Nogoya	CM2	795	7865	10.11	0.63	0.93	T I	1
144	Paris	CM2	579	7984	7.25	0.78	0.26	T I	0
149	Sutter's Mill	C	809	4127	19.6	0.81	0.25	III/T IV	...
28	LEW 85311	CM2-an	117	8199	1.43	0.58	0.04	T I	...
29	LEW 85312	CM2-an	231	10518	2.2	1.19	0.12	T I	...
41	PCA 91008	CM2-an	93	2055	4.53	1.78	0.01	III/T IV	...
42	QUE 93005	CM2-an	523	5009	10.44	0.72	0.49	T II	...
51	Yamato 81020	CO3.0	46	2678	1.72	0.03	4.33	LDH	...
49	Kainsaz	CO3.2	1066	12301	8.67	0.85	1.3	LDH	1
52	Yamato 82050	CO3.2	1340	14582	9.19	1.16	0.78	LDH	...
50	Yamato 791717	CO3.3	1093	16326	6.69	0.77	1.55	LDH	1
53	Yamato 82094	CO3.5	386	4153	9.29	0.35	1.17	LDH	2
54	GRO 95577	CR1	695	4371	15.9	1.48	0.22	T I	...
55	EET 92042	CR2	396	10019	3.95	0.36	0.7	T I	...
56	GRA 06100	CR2	1086	5386	20.16	1.77	0.93	III/T IV	...
58	GRO 03116	CR2	144	2026	7.11	0.26	1.91	III/T IV	...
59	MET 00426	CR2	540	7075	7.63	0.62	1.46	T I	...
60	QUE 99177	CR2	729	14523	5.02	0.64	0.7	T I	...
11	Allende	CV3	509	4918	10.35	0.4	2.31	LDH	...
169	Kaba	CV3	494	5611	8.8	0.37	0.67	T I	...
1	Aba Panu	L3	433	5723	7.57	0.22	1.62	LDH	4
180	Renchen	L5-6	1249	9917	12.59	0.53	2.4	LDH	4
12	Battle Mountain	L6	656	11032	5.95	0.56	1.68	LDH	4
16	Braunschweig	L6	829	4708	17.61	1.25	1.17	LDH	4
93	Novato	L6	1673	11229	14.9	1.48	1.37	LDH	4
151	Soltmany	L6	501	7699	6.51	0.55	3.83	LDH	2
157	Vicencia	LL3.2	304	5411	5.62	0.24	2.04	LDH	1
20	Chelyabinsk	LL5	2266	14667	15.45	1.69	0.96	LDH	4
181	Stutenberg	LL6	828	5988	13.83	0.69	1.4	LDH	3

Note. Where data on heating history are present, the samples were used for the PLS-DA of Figure 5 (Krot et al. 2019).

PLS-DA regression models are supervised models applied to find the best separation among samples (Wold et al. 2001). Therefore, we used the three above-mentioned groups to perform the PLS-DA analysis. The intensities of the CHOSMg compounds and the frequency are the basis for the calculation of the loadings. Specific loadings are representative for each of the three groups. The highest loading values, and hence the most representative

CHOSMg compounds, were extracted to show which compounds describe each of the groups the best (Ruf et al. 2017). For the model in Figure 5, we extracted three groups of loadings, namely, for the T I group (in dark blue), the T II and T III/T IV group (in light red), and the LDH group (in dark red).

To evaluate the meteorite data, we used a PLS-DA regressions model with the sevenfold cross-validation procedure. $R^2(Y)$ and

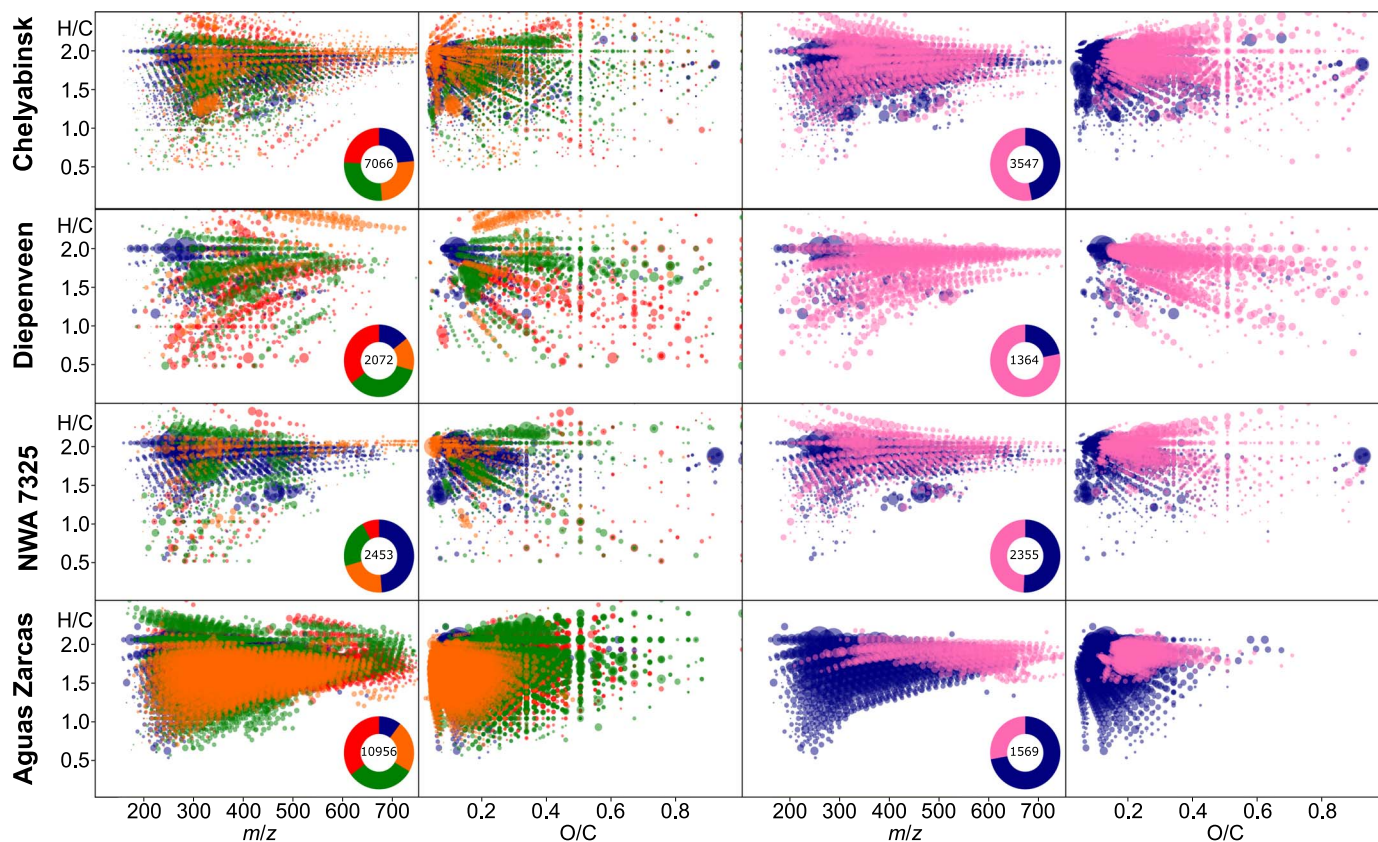


Figure A1. Depicted are mass-edited H/C ratio diagrams (left side of each of the two panels) and O/C ratio vs. H/C ratio (van Krevelen) diagrams (right side of each of the two panels) of the four meteorites from Figure 1. Bubble size represents the intensity in the mass spectrum; color represents the chemical space. CHO = blue, CHNO = orange, CHOS = green, CHNOS = red, CHOMg = magenta. The donut plot shows the total amount of each of the chemical spaces according to the color code as described in this legend.

$Q^2(\text{cum})$ values are reported to show the goodness of the fit and the quality of the prediction and to exclude possible overfitting.

The model of the PLS-DA in Figure 5 was built with two significant components, with $R^2(Y) = 0.49$ and $Q^2(\text{cum}) = 0.24$. Three groups were chosen according to information as found in Table A1. The p -value < 0.0001 confirms the robustness of the classification.

The PLS-DA analysis was built with SIMCA-P (Version 9.0, 2001 July 12, Umetrics AB). Figures were built in Python 3.8.5 within the Jupyter Notebook environment of Anaconda Version 1.9.7.

A.7. Calculations

To calculate weighted averages of a descriptive ratio (e.g., H/C or O/C), each value of each assignment is multiplied by its intensity. The sum of these new values is then divided by the sum of all intensities to get the weighted average value. By this operation, the values of more intense peaks are weighted more than those of less intense peaks.

Double bond equivalents are a number to describe how many double bonds a molecule potentially has. $\text{DBE} = \text{C} + 1 - (\text{H}/2) + (\text{N}/2)$ (Bae et al. 2011).

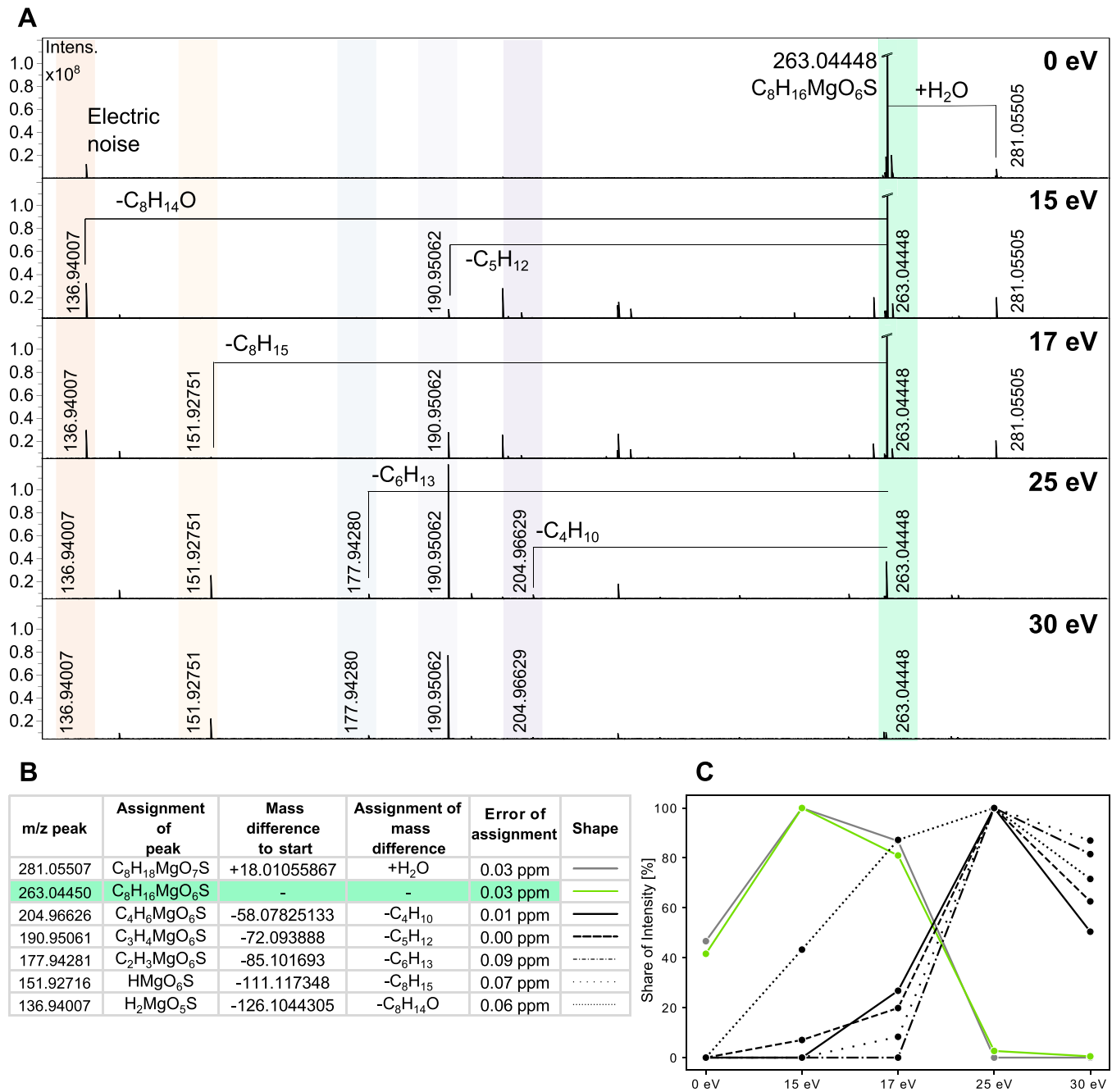


Figure A2. MS/MS experiments of CHOSMg compounds. (A) (-) ESI-FT-ICR-MS spectra of methanolic extract of Nogoya meteorite. Quadrupole Q1 mass was set to m/z 263 to isolate m/z 263.04448, which is annotated as C₈H₁₆MgO₆S. Spectra with different electron volt (eV) voltage is displayed. At 15 eV, fragments of charge remote fragmentations can be observed, while the intensity of the CHOSMg decreases. (B) All annotated peaks belonging to the initial isolated peak. Only the carbon chain is shortened by charge remote fragmentation, showing the high stability of the magnesium-sulfur head group. Loss of SO₂, SO₄, MgO₄S, or MgO₆S were not observed. (C) Intensity of all detected fragment peaks in the MS/MS measurements. A decrease of the isolated peak can be observed, while the fragmentation results in an increase in intensity. Ultimately, all peaks decrease in intensity at high voltage.

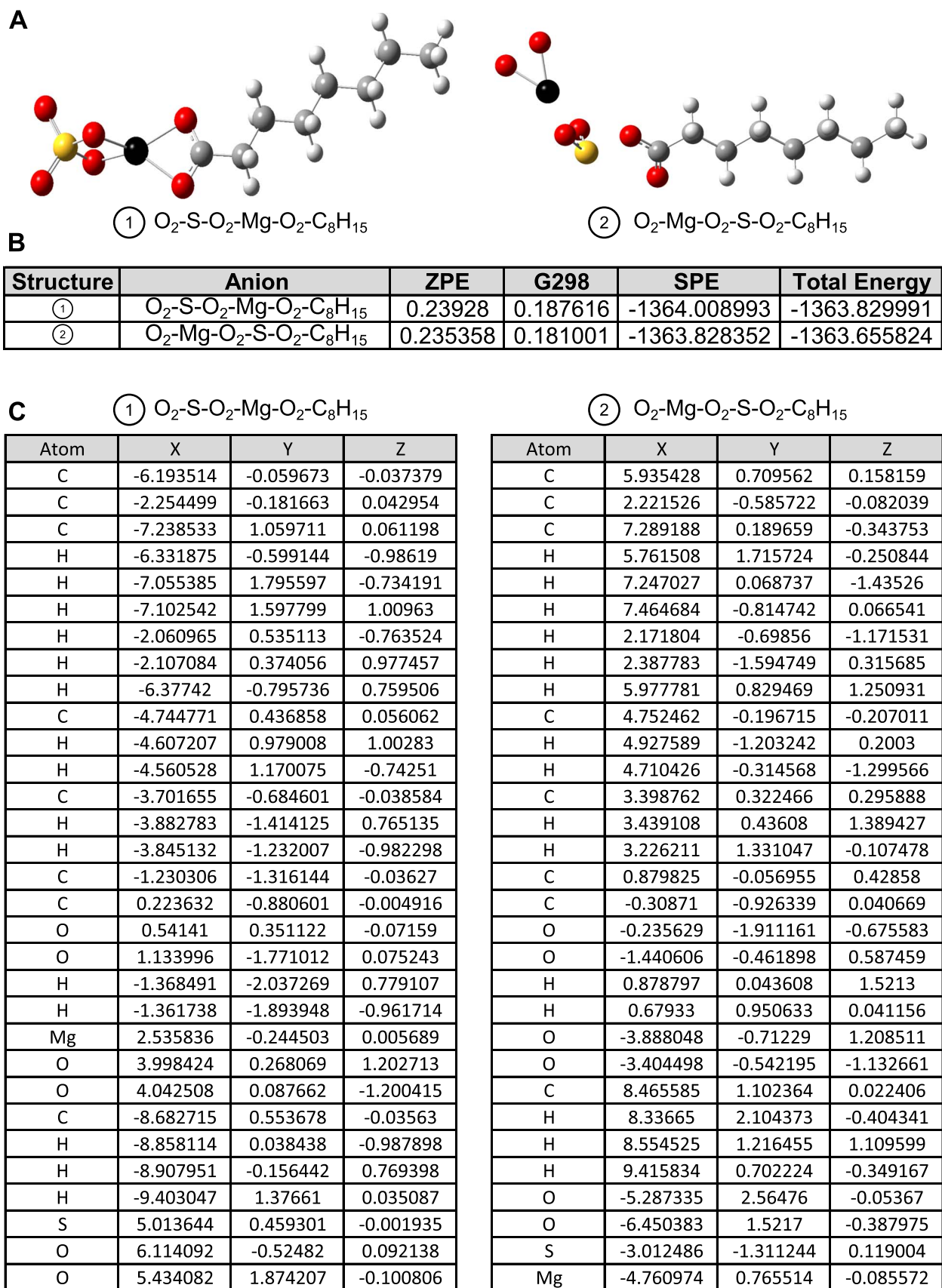


Figure A3. (A) According to MS/MS results as seen in Figure A2, two different possible chemical structures were tested for their stability. (B) Gas-phase total energy difference (ΔG) between $\text{O}_2\text{C}_8\text{H}_{15}\text{OOMgSO}_4$ and $\text{O}_2\text{C}_8\text{H}_{15}\text{OOSO}_2\text{MgO}_2$ anions were calculated. The zero-point vibrational energy (ZPE) and the Gibbs free energy at room temperature $T = 298\text{ K}$ (G298) were calculated on the B3LYP/6-31+G(d,p) level of theory and given in Hartrees. The single-point energy (SPE) was calculated at a higher 6-311+G(d,p) level of theory and is given in Hartrees. The energy difference between both anions is $109.3\text{ kcal mol}^{-1}$. (C) XYZ coordinates of the proposed two anions in their relaxed geometry.

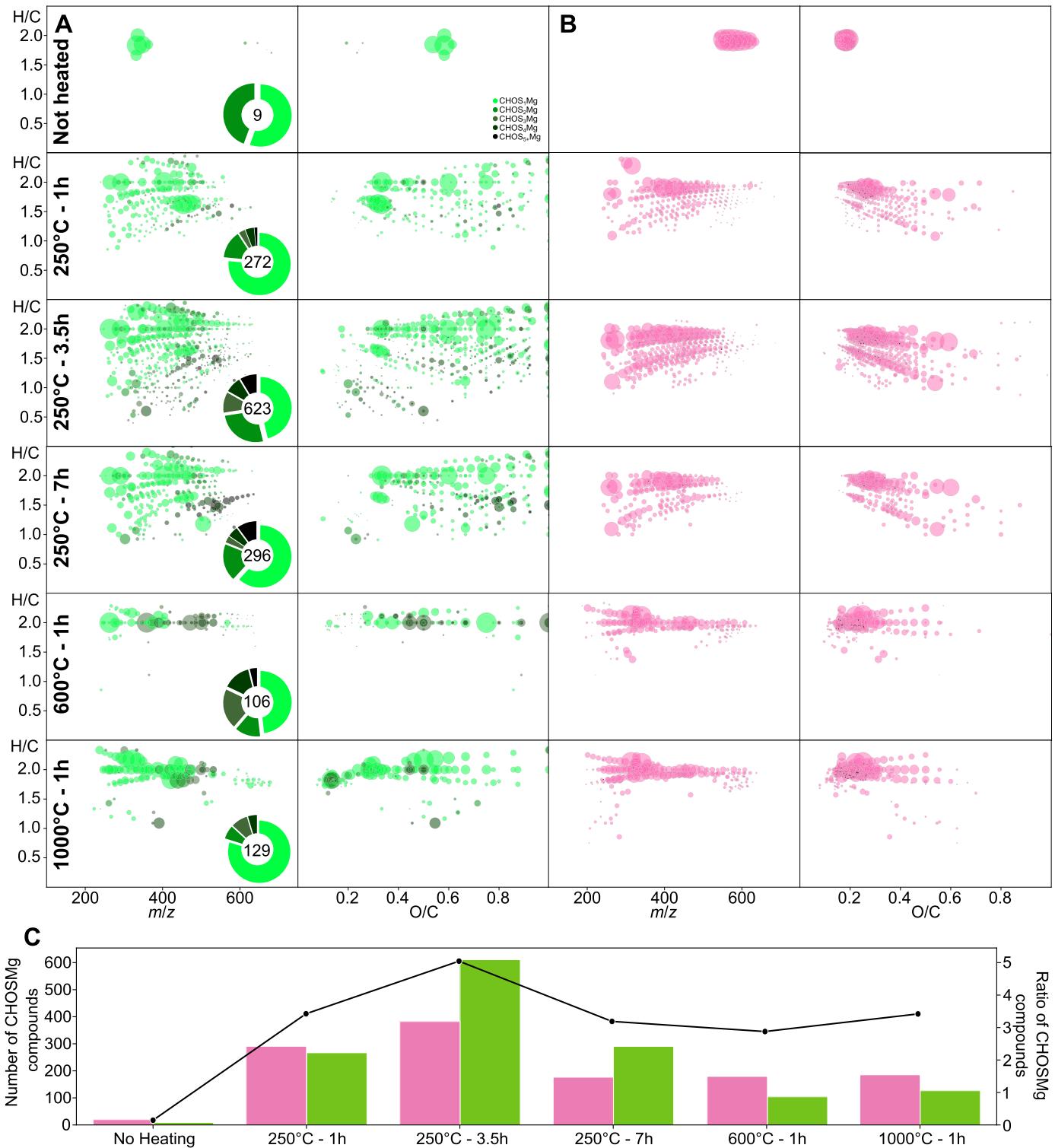


Figure A4. Heating experiment with Murchison meteorite. Similar-sized fragments of Murchison Meteorite were heated to 250°C for different durations, and also to 600°C and 1000°C for 1 hr. Depicted are mass-edited H/C ratio diagrams and O/C ratio vs. H/C ratio (van Krevelen) diagrams of (A) CHOSMg compounds (left side in green) and (B) CHOMg compounds (right side in magenta). Bubble size represents the intensity in the mass spectrum; color represents the amount of sulfur per CHOSMg compound according to the legend in the left panel. An increase of CHOSMg compounds and CHOMg compounds with higher temperatures and heating duration can be observed. (C) Absolute amount of CHOSMg compounds (green bar charts) and CHOMg compounds (magenta bar charts) for each of the six measurements (left Y-axis) and ratio of CHOSMg compounds to all measured compounds (line plot) to all measured compounds (right Y-axis) are shown. Absolute amount of CHOSMg compounds and the ratio increase with temperature but decrease again with very high temperature. CHOMg compounds increase with temperature and are more stable at the highest temperatures than CHOSMg compounds.

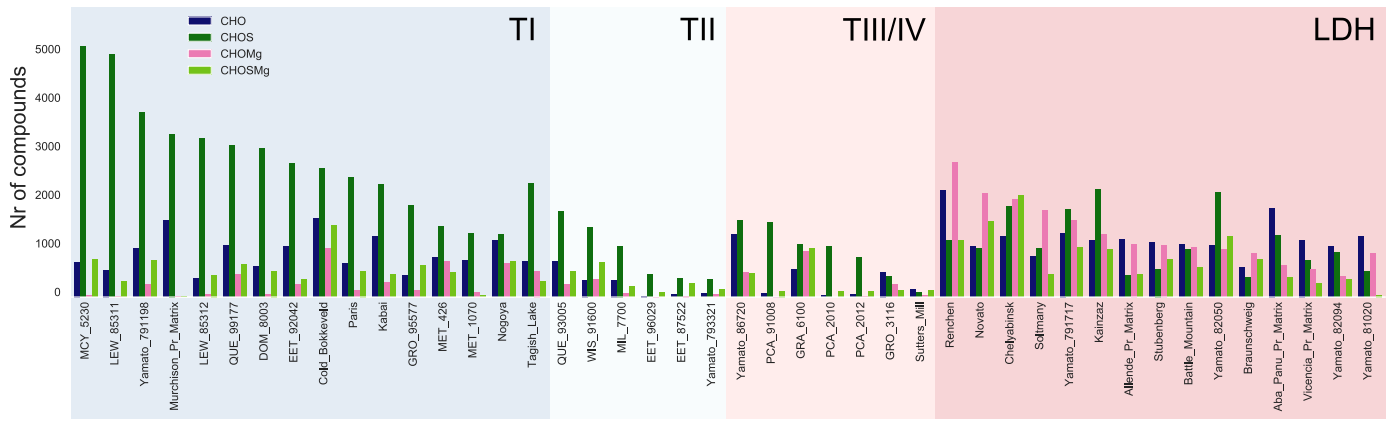


Figure A5. Barchart with the total amount of CHO (blue), CHOS (dark green), CHOMg (magenta), and CHOSMg (light green). Lower heated samples are more to the left, and higher heated samples are placed more to the right. Information on the samples can be found in Table A1.

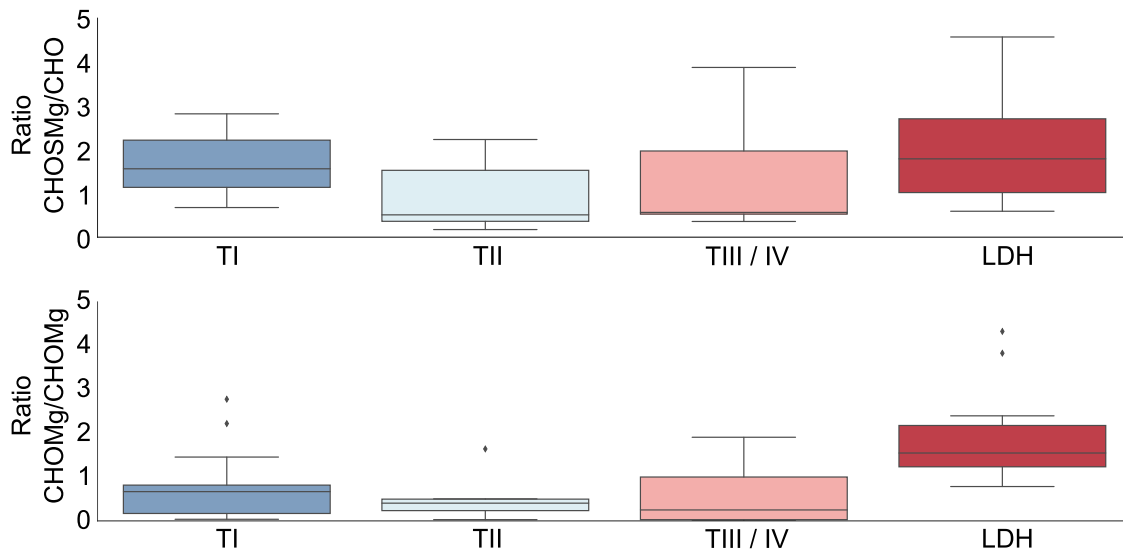


Figure A6. Boxplots of the ratio of CHOSMg to CHO compounds (top chart) and of the ratio of CHOMg to CHOSMg compounds (bottom chart) of the respective meteorites as seen in Table A1.

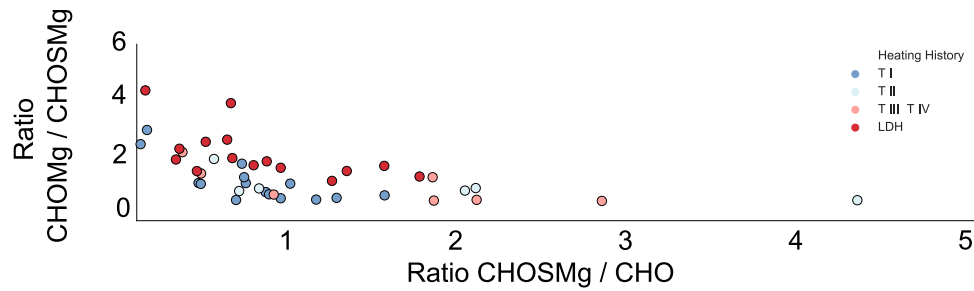


Figure A7. Scatterplot of ratios of CHOSMg to CHO (X-axis) and of CHOMg to CHOSMg (Y-axis) of the respective meteorites as seen in Table A1.

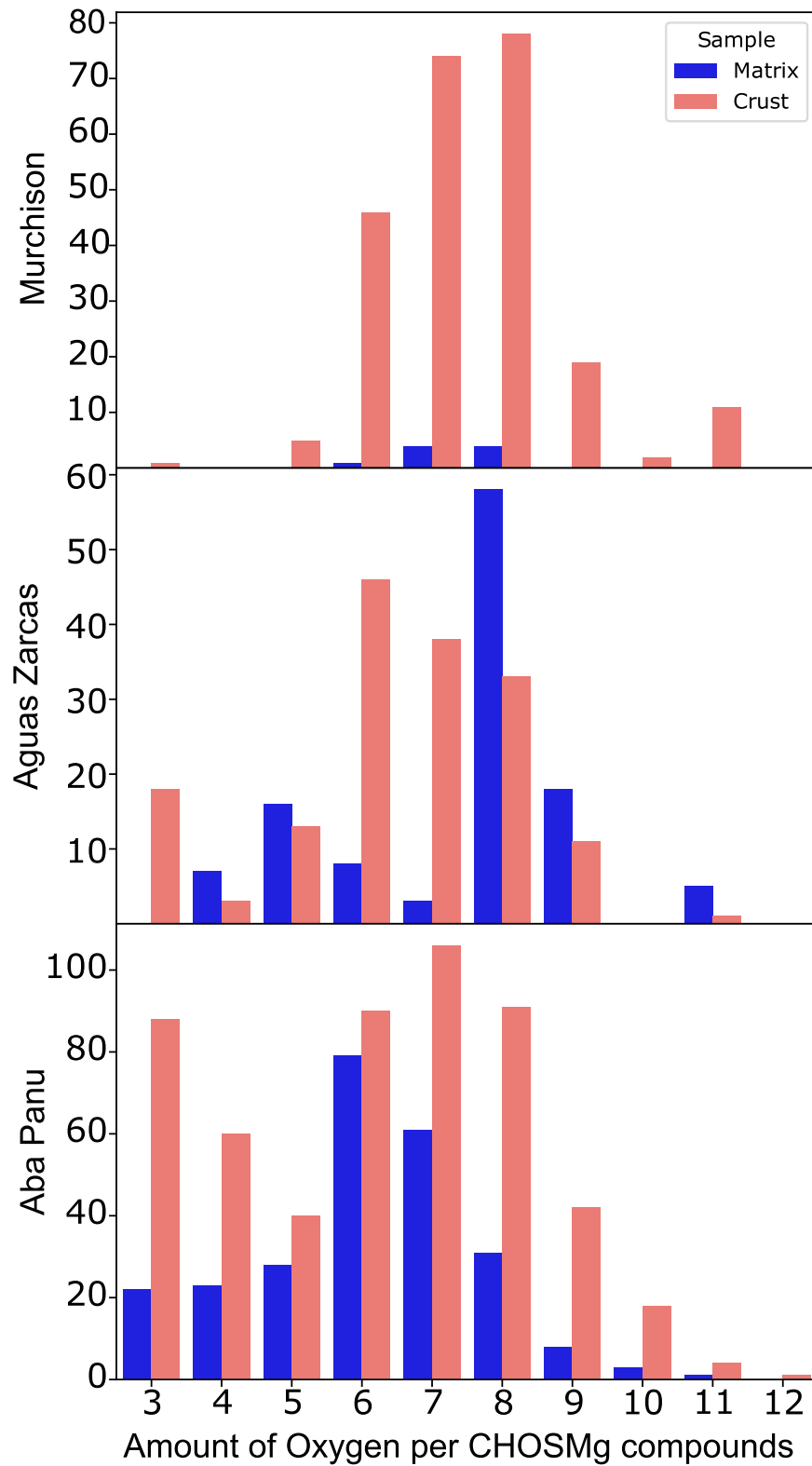


Figure A8. Detailed view of Figure 4 in the main text. All three meteorites are depicted by different bar charts. Amounts of CHOSMg compounds in matrix (blue bars) and in crust (red bars) are depicted on the Y-axis; amounts of oxygen per CHOSMg compounds are depicted on the X-axis.

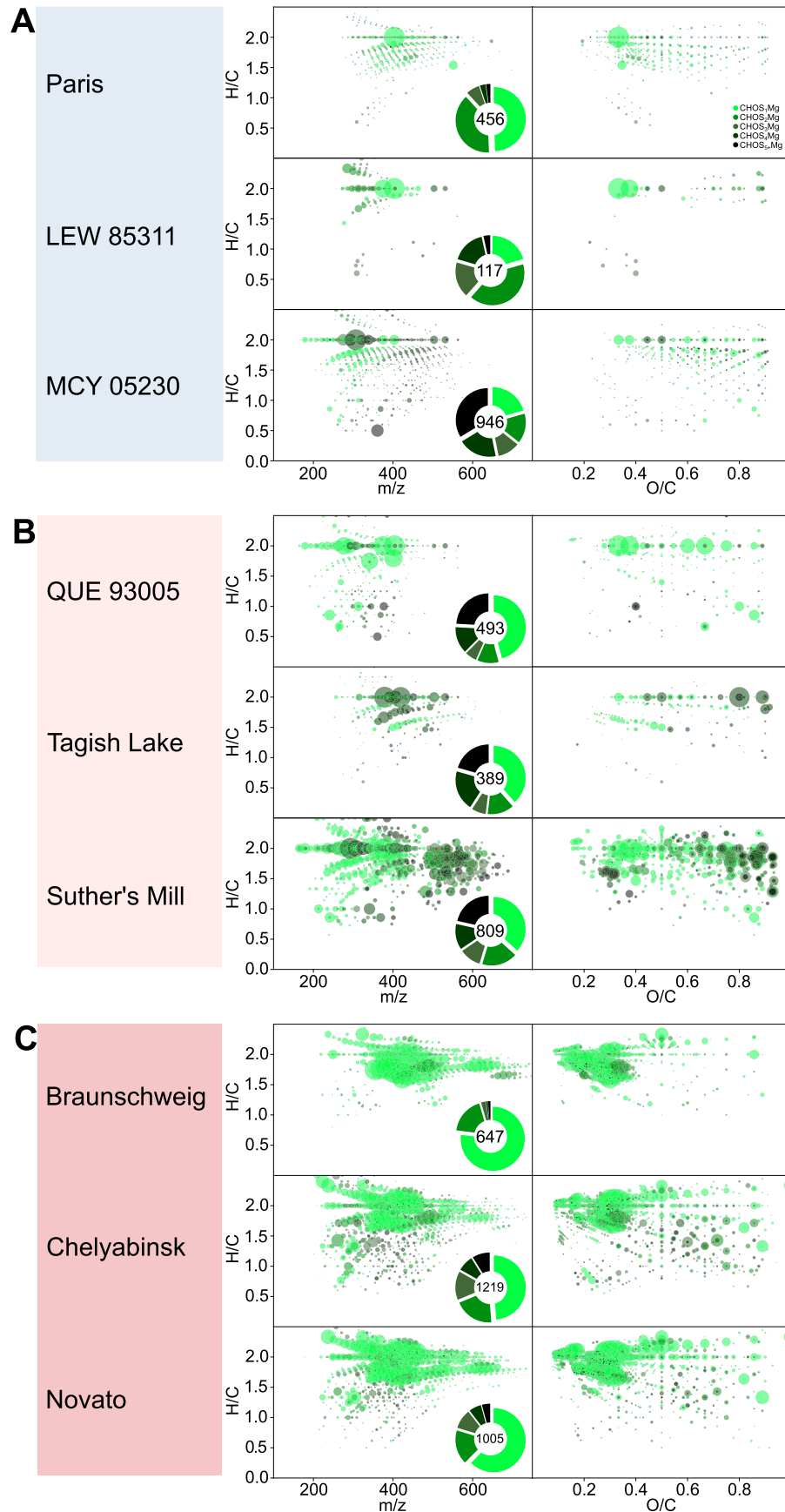


Figure A9. Detailed view of selected meteorites from the PLS-DA of Figure 5 in the main text. (A) Three meteorites from the T I heated ones. (B) Three meteorites from the T II and T III/T IV. (C) Three meteorites from the long-duration heating. Depicted are mass-edited H/C ratio diagrams (left side of each of the six panels) and O/C ratio vs. H/C ratio (van Krevelen) diagrams (right side of each of the six panels). Bubble size represents the intensity in the mass spectrum; color represents the amount of sulfur per CHOSMg compound according to the legend.

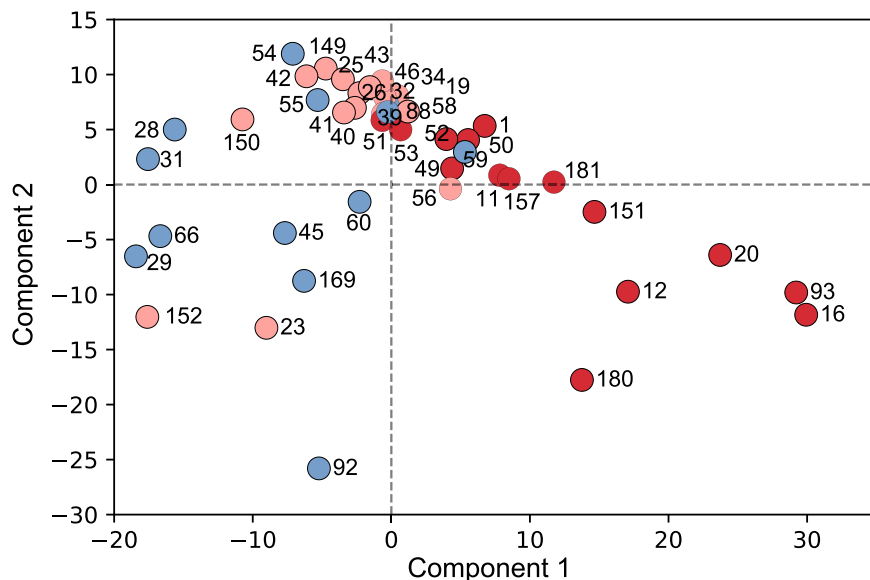


Figure A10. PCA of similar data is found in the PLS-DA in Figure 5. PCA of 44 different well-described meteorites according to their thermal metamorphism history. Only CHOSMg compounds were used as PCA loadings. Three categories were chosen according to the assigned thermal history. Hydrothermal background without short-duration heating (T I; dark blue), moderate short-duration heating (T II) and intense short-duration heating (T III/T IV; light red), and long-duration heating (LDH; dark red). Information on samples can be found in Table A1.

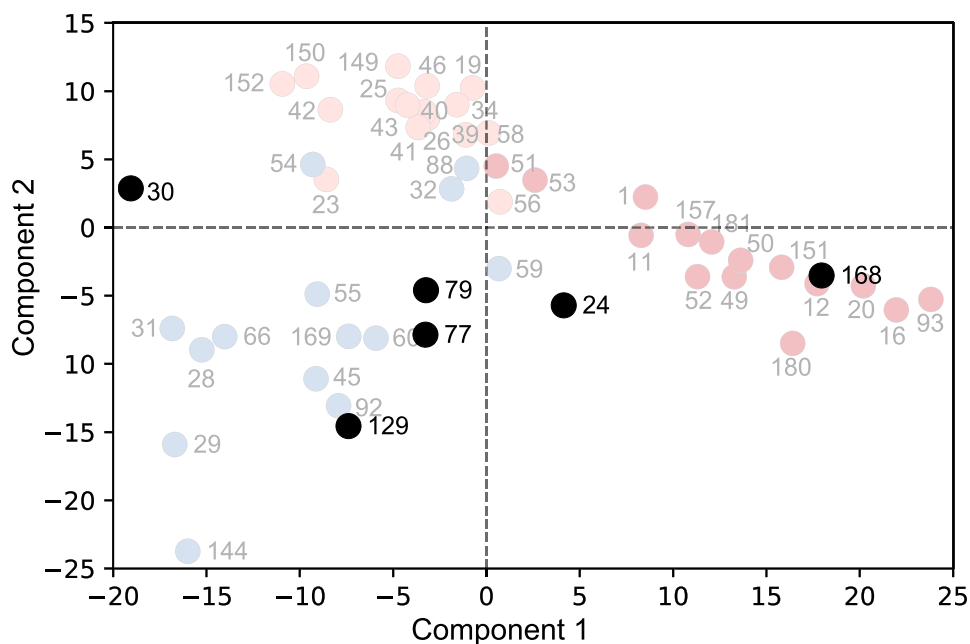


Figure A11. Prediction with the PLS-DA from Figure 5. The PLS-DA model was used to predict the positioning of samples that were not classified in the T I, T II, T III/IV LDH system yet. Classified samples are Orgueil (129—CI), Ivuna (77—CI), Mukundpura (79 CM2), Maribo (30—CM2), Diepenveen (24—CM2-an), and Dhofar 1988 (168—CM2-an). The CI meteorites Orgueil and Ivuna have seen almost hardly any heat; thus, their CHOSMg signature is similar to those of T I meteorites. Maribo and Mukundpura are more similar to Murchison and thus move away from T I meteorites more into the direction of T II and T III/IV meteorites. Diepenveen and Dhofar 1988 both experienced some heating; thus, their CHOSMg signatures cluster them to LDH meteorites. Dhofar 1988 especially was recently reclassified as CY and shows subsequent thermal alteration (Suttle et al. 2021), which is also corroborated by the positioning with the LDH meteorites in the PLS-DA.

ORCID iDs

Philippe Schmitt-Kopplin  <https://orcid.org/0000-0003-0824-2664>

References

- Anders, E. 1971, *ARA&A*, **9**, 1
- Aponte, J. C., McLain, H. L., Simkus, D. N., et al. 2020, *M&PS*, **55**, 1509
- Bae, E., Yeo, I. J., Jeong, B., et al. 2011, *AnaCh*, **83**, 4193
- Bonal, L., Quirico, E., Flandinet, L., & Montagnac, G. 2016, *GeCoA*, **189**, 312
- Botta, O., & Bada, J. L. 2002, *SGeo*, **23**, 411
- Callahan, M. P., Smith, K. E., Cleaves, H. J., et al. 2011, *PNAS*, **108**, 13995
- Cronin, J. R., & Pizzarello, S. 1983, *AdSpR*, **3**, 5
- Dennington, R., Keith, T., Millam, J., et al. 2003, GaussView, Version 5.0.8, Semichem Inc., Shawnee Mission, KS
- Furukawa, Y., Chikaraishi, Y., Ohkouchi, N., et al. 2019, *PNAS*, **116**, 24440
- Gattacceca, J., Mccubbin, F. M., Bouvier, A., & Grossman, J. 2020, *M&PS*, **55**, 460
- Hashiguchi, M., & Naraoka, H. 2019, *M&PS*, **54**, 452

- Hertkorn, N., Frommberger, M., Witt, M., et al. 2008, [AnaCh](#), 80, 8908
- Hertkorn, N., Harir, M., & Schmitt-Kopplin, P. 2015, [Magn Reson Chem](#), 53, 754
- Hertzog, J., Naraoka, H., & Schmitt-Kopplin, P. 2019, [Life](#), 9, 48
- Kaplan, I. R., & Hulston, J. R. 1966, [GeCoA](#), 30, 479
- Krot, A. N., Nagashima, K., Fintor, K., & Pál-Molnár, E. 2019, [GeCoA](#), 246, 419
- Kvenvolden, K. A., Lawless, J. G., & Ponnamperna, C. 1971, [PNAS](#), 68, 486
- Langbroek, M., Jenniskens, P., Kriegsman, L. M., et al. 2019, [M&PS](#), 54, 1431
- Lauretta, D. S., & McSween, H. Y. 2006, *Meteorites and the Early Solar System II* (Tucson, AZ: Univ. Arizona Press)
- Lawless, J. G., & Yuen, G. U. 1979, [Natur](#), 282, 396
- Leonzio, G. 2016, [Chem Eng J](#), 290, 490
- Marianna, L., Fekete, A., Frommberger, M., & Schmitt-Kopplin, P. 2011, in *Handbook of Molecular Microbial Ecology I: Metagenomics and Complementary Approaches*, ed. F. J. de Bruijn (New York: Wiley), 683
- Martins, Z., Botta, O., Fogel, M. L., et al. 2008, [E&PSL](#), 270, 130
- Masters, C. 1979, [Adv. Organomet. Chem.](#), 17, 61
- McGeoch, M., Dikler, S., & McGeoch, J. E. 2020, arXiv:2002.11688
- Naraoka, H., Yamashita, Y., Yamaguchi, M., & Orthous-Daunay, F.-R. 2017, [ESC](#), 1, 540
- Orthous-Daunay, F.-R., Quirico, E., Lemelle, L., et al. 2010, [E&PSL](#), 300, 321
- Pizzarello, S., Cooper, G., & Flynn, G. 2006, in *Meteorites and the Early Solar System II*, ed. D. S. Lauretta & H. Y. McSween, Jr. (Tucson, AZ: Univ. Arizona Press), 625
- Popova, O. P., Jenniskens, P., Emel'yanenko, V., et al. 2013, [Sci](#), 342, 1069
- Quirico, E., Bonal, L., Beck, P., et al. 2018, [GeCoA](#), 241, 17
- Quirico, E., Orthous-Daunay, F.-R., Beck, P., et al. 2014, [GeCoA](#), 136, 80
- Ruf, A., Kanawati, B., Hertkorn, N., et al. 2017, [PNAS](#), 114, 2819
- Sabatier, P. 1913, *La catalyse en chimie organique* (Paris et Liege: Librairie Polytechnique)
- Schmitt-Kopplin, P., Gabelica, Z., Gougeon, R. D., et al. 2010, [PNAS](#), 107, 2763
- Sears, D. 1975, *ModGe*, 5, 155
- Smith, D. F., Podgorski, D. C., Rodgers, R. P., Blakney, G. T., & Hendrickson, C. L. 2018, [AnaCh](#), 90, 2041
- Smith, K. E., House, C. H., Arevalo, R. D., Dworkin, J. P., & Callahan, M. P. 2019, [NatCo](#), 10, 2777
- Srinivasan, B., & Anders, E. 1978, [Sci](#), 201, 51
- Summons, R. E., Albrecht, P., McDonald, G., & Moldowan, J. M. 2008, [SSRv](#), 135, 133
- Suttle, M. D., Greshake, A., King, A. J., et al. 2021, [GeCoA](#), 295, 286
- Tenailleau, C., Etschmann, B., Ibberson, R. M., & Pring, A. 2006, [AmMin](#), 91, 1442
- Toppani, A., Libourel, G., Engrand, C., & Maurette, M. 2001, [M&PS](#), 36, 1377
- Unsalan, O., Jenniskens, P., Yin, Q.-Z., et al. 2019, [M&PS](#), 54, 953
- Van Krevelen, D. W. 1950, *Fuel*, 29, 269
- Van Schmus, W. R., & Wood, J. A. 1967, [GeCoA](#), 31, 747
- Wakil, S. J. 1989, [Biochemistry](#), 28, 4523
- Wold, S., Sjöström, M., & Eriksson, L. 2001, [Chemom. Intell. Lab. Syst.](#), 58, 109